Received: 21 August 2025 | Revised: 21 October 2025 | Accepted: 26 October 2025

DOI: 10.1002/ijgo.70650

CLINICAL ARTICLE

Gynecology

A sex-informed transcriptomic prognostic score for gynecologic cancers: Multiplatform validation and spatial characterization

Mauricio A. Cuello[1,2,3] | Fernán Gómez-Valenzuela[4] | Ignacio Wichmann[5,6] | Sumie Kato[1] | Carolina Ibañez[7]

[1]Department of Gynecology, School of Medicine, Pontificia Universidad Católica de Chile (PUC), Santiago, Chile

[2]Gynecologic Oncology Unit, Hospital Clínico Universidad Católica, UC-Christus Health Network, Santiago, Chile

[3]Center for Cancer Prevention and Control (CECAN), Santiago, Chile

[4]Precision Oncology Center, School of Medicine, Universidad Mayor, Santiago, Chile

[5]Department of Obstetrics, School of Medicine, Pontificia Universidad Católica de Chile (PUC), Santiago, Chile

[6]Division of Oncology, Department of Medicine, Stanford University School of Medicine, Stanford, California, USA

[7]Department of Hematology and Oncology, School of Medicine, Pontificia Universidad Católica de Chile (PUC), Santiago, Chile

Correspondence
Mauricio A. Cuello, Department of Gynecology, School of Medicine, Pontificia Universidad Católica de Chile, Diagonal Paraguay 362, Santiago, 8330077, Chile.
Email: mcuello@uc.cl

Funding information
ANID/FONDAP, Grant/Award Number: 152220002

Abstract

Objective: This study develops and validates a sex-informed transcriptomic prognostic score derived from sex-stratified survival analyses, with a focus on gynecologic malignancies.

Methods: This retrospective, computational multi-cohort study analyzed transcriptomic and clinical data from The Cancer Genome Atlas (TCGA; $n \approx 5000$) and CPTAC-3 ($n = 2191$). A 10-gene score was constructed using sex-stratified Cox models and LASSO regression across 20 TCGA tumor types. Prognostic performance was evaluated using hazard ratios and time-dependent AUCs at 1, 3, and 5 years. Analyses followed a four-phase design: discovery in TCGA, internal cross-cancer validation, external validation in independent cohorts (MSK-IMPACT, CPTAC-3, and LIHC-FR), and biological validation using single-cell and spatial transcriptomic data from formalin-fixed paraffin-embedded tissues. Patients were stratified into high- and low-risk groups based on the median gene-expression score, with optimal cutpoints determined using maximally selected rank statistics where indicated. While the discovery analyses were sex-stratified, the final 10-gene score is sex-agnostic and applicable to both sexes.

Results: The score showed strong prognostic discrimination (hazard ratio = 2.15; 95% confidence interval 1.60–2.88; $P < 0.001$), with areas under the curve ranging from 0.69 to 0.72 across timepoints. It remained robust across datasets and analytic platforms. In gynecologic tumors, high-score regions colocalized with fibroblast-rich, immune-depleted areas, reflecting transcriptional programs of stromal remodeling and immune exclusion linked to immunotherapy resistance.

Conclusion: This sex-informed, spatially validated score provides a reproducible and biologically interpretable framework for transcriptomic risk stratification in gynecologic cancers. By capturing immune-evasive and aggressive tumor states, it might inform biomarker-guided clinical trials and support context-appropriate implementation of precision oncology strategies.

KEYWORDS
biomarkers, cohort studies, gene expression profiling, gynecologic neoplasms, prognosis, sex characteristics, transcriptome, tumor microenvironment

1 | INTRODUCTION

Sex-based differences in cancer biology and outcomes are well established,[1–3] with male patients showing poorer prognosis across several malignancies, including lung, liver, and colorectal cancers, even after adjustment for known factors.[4,5] Despite this, most predictive models remain sex-agnostic, neglecting sex-specific molecular traits that shape prognosis and treatment response.[6–8]

Publicly available cancer datasets, such as The Cancer Genome Atlas (TCGA), CPTAC, MSK-IMPACT, and GEO, offer powerful opportunities to investigate sex-specific prognostic patterns.[9,10] Recent transcriptomic analyses have revealed sex-related gene expression programs involved in immune surveillance, metabolism, and cell cycle control,[11,12] yet these insights have rarely been translated into clinically actionable tools, especially in gynecologic cancers, where immunotherapy efficacy remains limited and predictive biomarkers inconsistent.[13–15]

This clinical gap underscores the need for prognostic tools that not only capture sex-related molecular traits but also reflect spatial immune dynamics and tumor microenvironmental features relevant to therapeutic response. In gynecologic cancers, sex-linked hormonal, immune, and genetic influences modulate tumor biology and response to therapy, further justifying sex-aware biomarker discovery.

In this study, we derived and validated a 10-gene sex-informed prognostic score using an integrative, multi-platform approach, including bulk RNA-seq, single-cell, and spatial transcriptomics. While validating pan-cancer, our focused application in endometrial, ovarian, and cervical cancers assessed its relevance in tumor architecture and immune contexture.

High-score tumors showed enrichment in transcriptional programs linked to immune suppression and stromal remodeling (e.g., natural killer (NK)-cell depletion and T-cell exclusion), features associated with resistance to immune checkpoint inhibitors. This suggests the score could help identify immunotherapy-resistant gynecologic tumors or guide combinatorial strategies. Importantly, this information could be leveraged in formalin-fixed paraffin-embedded (FFPE) samples using platforms such as NanoString or reverse transcription-quantitative polymerase chain reaction (RT-qPCR), expanding the score's clinical applicability beyond research settings.

Currently, PD-L1 IHC and molecular subtype are used to predict response but with limited consistency in gynecologic cancers.[16–21] Our transcriptomic score offers a spatially informed, immune-contextual tool that might refine treatment strategies independently of PD-L1 status, linking biological sex, tumor-intrinsic aggressiveness, and microenvironmental features to inform biomarker development and clinical decision-making. Its consistent performance across transcriptomic platforms and tumor types supports its potential for integration into real-world gynecologic oncology workflows, aiding treatment selection and improving personalized care.

2 | MATERIALS AND METHODS

2.1 | Data sources and integrative analytical framework

This retrospective, computational study analyzed publicly available cancer datasets covering cases collected between 2013 and 2024. Discovery used TCGA pan-cancer cohorts (≈5000 samples across 20 tumor types), where sex-stratified Cox analyses were performed within each tumor type. Internal validation was conducted across these 20 TCGA tumor types. External validation included MSK-IMPACT ($n = 1514$), CPTAC-3 ($n = 2191$), and LIHC-FR ($n \approx 1000$). Biological validation incorporated 33 single-cell RNA-seq and four FFPE spatial transcriptomic samples. The workflow comprised four sequential phases: (1) discovery using sex-stratified survival analyses in TCGA pan-cancer cohorts; (2) internal validation across 20 TCGA tumor types; (3) external validation using independent cohorts (MSK-IMPACT, CPTAC-3, and LIHC-FR); and (4) biological and spatial validation integrating single-cell and FFPE 10× Visium data. Figure 1 summarizes the study design, datasets, sample sizes, and analytical sequence.

This study constitutes a secondary analysis of publicly available cancer datasets, integrating retrospective bioinformatic pipelines to identify sex-related prognostic patterns. The overarching goal was to develop a clinically translatable prognostic tool that integrates sex-specific molecular signals and spatial immune contexture to guide risk stratification.

The primary discovery dataset was The Cancer Genome Atlas (TCGA), encompassing RNA-sequencing and survival data from the 10 most prevalent solid tumors. Model validation was conducted across 20 cancer types internally, and externally in the MSK-IMPACT cohort ($n = 1514$),[22] the CPTAC-3 proteogenomic dataset (NCI CPTAC, dbGaP accession: phs001287.v5.p4), and a European hepatocellular carcinoma cohort (LIHC-FR).[23] All data were accessed via UCSC Xena,[24] cBioPortal,[25,26] and 10× Genomics repositories.

All datasets were previously collected under institutional review board approval with informed consent as part of TCGA, CPTAC, MSK-IMPACT, and other publicly funded projects. No new human subjects were recruited.

2.2 | Identification of sex-specific prognostic genes

We performed sex-stratified univariable Cox models using *Z*-score–normalized gene expression to identify genes associated with overall survival (OS) and progression-free interval (PFI). Candidates were retained if they showed significant (or trend-level, $P < 0.10$) association in one sex only or opposite hazard directions between sexes.

We used ToPP,[27] SmulTCan,[28] UALCAN,[29] and cBioPortal[30] for additional gene-level validation. *P*-values were adjusted using the Benjamini–Hochberg false-discovery-rate method with a threshold ≤0.10. Outputs and recurrence analyses are summarized in Tables S1–S4.

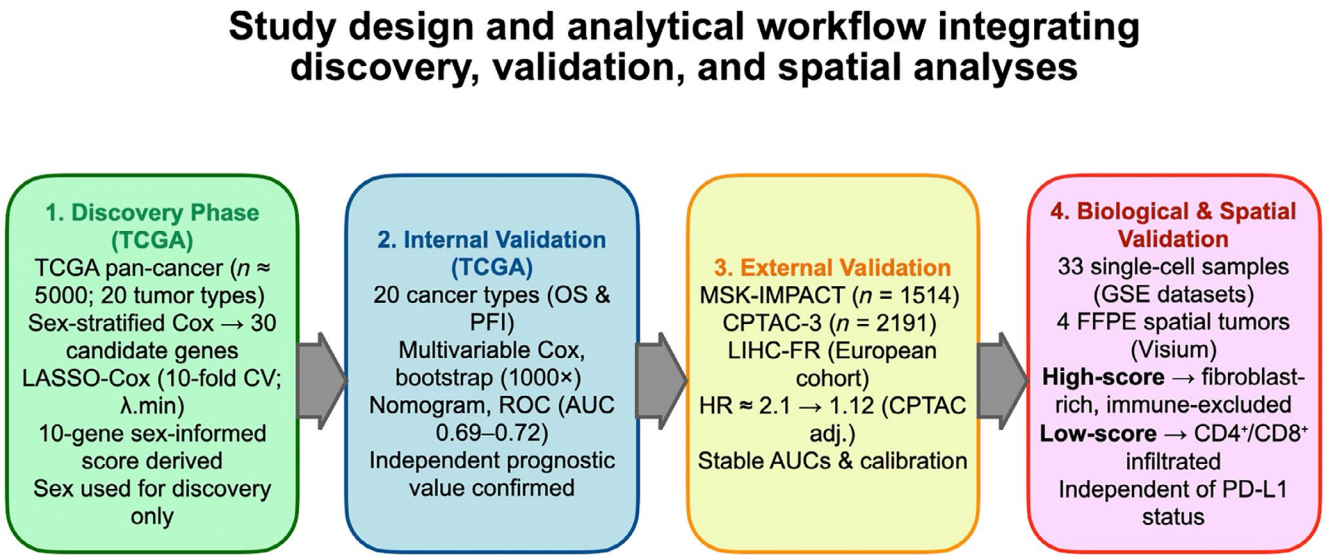

FIGURE 1 Study design and analytical workflow integrating discovery, validation, and spatial analyses. Step 1 (Discovery phase): Sex-stratified survival analysis across TCGA pan-cancer datasets identified genes with sex-biased prognostic effects for overall survival (OS) and progression-free interval (PFI). Step 2 (Internal validation): Multivariable Cox regression and bootstrap analyses confirmed the model's robustness across 20 tumor types. Step 3 (External validation): The 10-gene score was validated in independent cohorts (MSK-IMPACT, CPTAC-3, and LIHC-FR), showing stable discrimination and calibration. Step 4 (Biological and spatial validation): Single-cell and spatial transcriptomic datasets revealed that high-score regions were fibroblast-rich and immune-excluded, whereas low-score regions were $CD4^+$/$CD8^+$-infiltrated and independent of PD-L1 status. Retrospective computational analysis of publicly available datasets (2013–2025; TCGA, CPTAC, MSK-IMPACT, GEO), all originally collected under institutional ethics approval and informed consent. Boxes in the flow diagram indicate dataset and sample size per phase; arrows denote analytical sequence. Abbreviations: OS, overall survival; PFI, progression-free interval; TCGA, The Cancer Genome Atlas; CPTAC, Clinical Proteomic Tumor Analysis Consortium; MSK-IMPACT, Memorial Sloan Kettering–Integrated Mutation Profiling of Actionable Cancer Targets; GEO, Gene Expression Omnibus; FFPE, formalin-fixed paraffin-embedded.

2.3 | Construction of the prognostic score

Thirty genes were selected through the sex-stratified screen and entered into LASSO-penalized Cox regression to build a parsimonious model. Tenfold cross-validation determined the optimal penalty (lambda.min), and the final score was computed as a weighted linear combination of Z-standardized expression values.

Patients were stratified into high- and low-risk groups using the median gene expression score as the default cutpoint, with sensitivity analyses using maximally selected rank statistics (surv_cutpoint function, R package survminer v0.4.9[31]) to confirm the stability of risk group assignment. For spatial transcriptomics, a reduced version of the score was used to accommodate genes detectable in FFPE samples. This subset was optimized to ensure feasibility for clinical implementation using FFPE-compatible platforms such as NanoString or targeted RT-qPCR panels. Full annotations are presented in Table S5.

2.4 | Validation and clinical utility

Internal validation across 20 TCGA cancers was followed by external validation in MSK-IMPACT,[22] CPTAC-3,[23] and LIHC-FR cohorts. We assessed discrimination using time-dependent receiver operating characteristic (ROC) curves, Harrell's C-index, and nomogram calibration. Clinical value was evaluated via decision curve analysis (DCA) and net reclassification improvement (NRI).[32,33] These metrics assess the score's added value in clinical decision-making scenarios, beyond standard predictors like PD-L1 status or molecular subtype.

2.5 | Single-cell and spatial transcriptomic analyses

To characterize the tumor microenvironment, we analyzed 33 single-cell RNA-seq samples from gynecologic tumors and normal ovarian tissue, from datasets GSE165897, GSE154600, GSE197461, GSE168652, and GSE251923. Data were processed independently using Seurat v5.0 (RRID:SCR_007322). Malignant cells were identified via epithelial and oncogenic markers, and immune/stromal subsets via SingleR with BlueprintEncodeData.

Eight lineages were retained: $CD4^+$, $CD8^+$, NK, B cells, monocytes, fibroblasts, adipocytes, and malignant cells. UMAPs were used to visualize score distribution and immune checkpoint expression. Cell-type annotations were validated with TISCH2.[34]

Spatial transcriptomic data were obtained from FFPE samples of ovary, cervix, colorectal, and prostate tumors using the 10× Genomics Visium platform. Gene scores were computed per spot

and stratified into high- and low-risk regions. Co-localization with canonical markers ($CD4^+$, $CD8^+$, fibroblasts, and epithelial cells) was evaluated following FFPE spatial protocols[35] and analytic strategies used in gastrointestinal tumors.[36] The spatial mapping of the score supports its potential as a tissue-based biomarker for routine pathology workflows.

Spatial expression of CD274, PDCD1, and CTLA4 was compared across risk regions. For colorectal tumors, analyses were independently replicated.

2.6 | Functional and dependency analysis

Differential expression was analyzed with limma and moderated empirical Bayes methods; pathway enrichment was assessed via fgsea and clusterProfiler (Hallmark and Reactome pathways). Ecotype structure was deconvoluted using EcoTyper.[36]

Gene dependency was evaluated using CERES scores from DepMap 24Q4 (RRID:SCR_017655),[37] with group comparisons via Wilcoxon and Spearman tests.

2.7 | Gene annotation and novelty assessment

We evaluated oncogenic relevance by cross-referencing each gene with six major platforms: OncoKB,[38] COSMIC CGC,[39] MSK-IMPACT,[22] FoundationOne CDx,[40] Vogelstein's list,[41] and OncoMD.[42] A composite novelty index (0–6) was computed. Mutation–expression associations were explored using OncoMD.

2.8 | Statistical analyses

All analyses were conducted in R (version 4.3.2, R Foundation for Statistical Computing, Vienna, Austria) and SPSS Statistics (version 29.0, IBM; RRID:SCR_002865). Key packages included glmnet (v4.1-8) for LASSO-Cox regression, survival (v3.5-7), survminer (v0.4.9), rms (v6.7-0), clusterProfiler (v4.10), maxstat (v0.7-25), and Seurat (v5.1) for single-cell integration. Spatial transcriptomic preprocessing followed 10× Genomics Visium pipelines (Space Ranger v3.1). Univariable and multivariable Cox models were applied for survival analyses, with Kaplan–Meier curves and log-rank tests generated using survminer. Time-dependent ROC curves were computed with the timeROC package, and internal validation was performed via bootstrap resampling (1000 iterations).

Analyses were performed on complete-case data. The number of samples included in each discovery and validation dataset is indicated in the respective results subsections.

Nomograms were built using rms, calibration via decile-based plots, and DCA and NRI using rmda.[32,33]

All scripts and data used for score construction, visualization, and validation are available at: https://github.com/macuello1968/sex-informed-score.

2.9 | Availability of data and materials

All gene expression, clinical, and spatial datasets were obtained from public repositories: UCSC Xena, cBioPortal, 10× Genomics, and CPTAC-3 via dbGaP. No new data were generated. Key datasets include GSE108989 (colorectal), GSE141460 (glioma), GSE103322 (head and neck), GSE140228 (hepatocellular), and CPTAC-3 (phs001287.v5.p4).

Gynecologic single-cell datasets included GSE154600, GSE165897, GSE168652, and GSE251923. These covered high-grade serous, cervical, and endometrial tumors with epithelial and immune compartment resolution.

The inclusion of gynecologic tumors with epithelial and immune resolution supports future clinical testing of the score in diagnostic or predictive settings.

Detailed workflows are provided in Methods S1.

3 | RESULTS

3.1 | Sex-stratified survival discovery across common tumors

We first conducted sex-specific univariable Cox regressions across the 10 most prevalent solid tumors affecting both sexes, using *Z*-score–normalized gene expression for OS and PFI. Genes were prioritized if significant (or $P < 0.10$) in only one sex or showed opposite hazard directions.

To test generalizability, we extended analyses to sex-specific cancers, confirming strong performance in ovarian, endometrial, and cervical tumors. The final 10-gene panel was selected via LASSO-penalized Cox regression and independently applied to OS and PFI. Each gene was functionally linked to cancer hallmarks and retained consistent prognostic behavior. Sex guided discovery but was not included in the score formula, enabling cross-sex application. The discovery phase included approximately 5000 TCGA samples across 20 tumor types, followed by internal validation in the same cohorts, external validation in 3700 independent samples (MSK-IMPACT, CPTAC-3, and LIHC-FR), and biological validation in 33 single-cell and four FFPE spatial samples. This discovery phase established the foundation for the subsequent validation and spatial analyses described below.

In gynecologic cohorts specifically, univariable and multivariable Cox models remained significant after adjustment for stage and histology (Table S3).

3.2 | Pan-cancer validation of the 10-gene score

The score was evaluated in 28 TCGA cohorts for OS and 23 for PFI, including gynecologic cancers. Kaplan–Meier analyses showed robust separation of risk groups (Figure 2a,b), and multivariable Cox models yielded significant hazard ratios, exceeding 2.0 in pancreatic, endometrial, and adrenocortical cancers (Figure 2c,d).

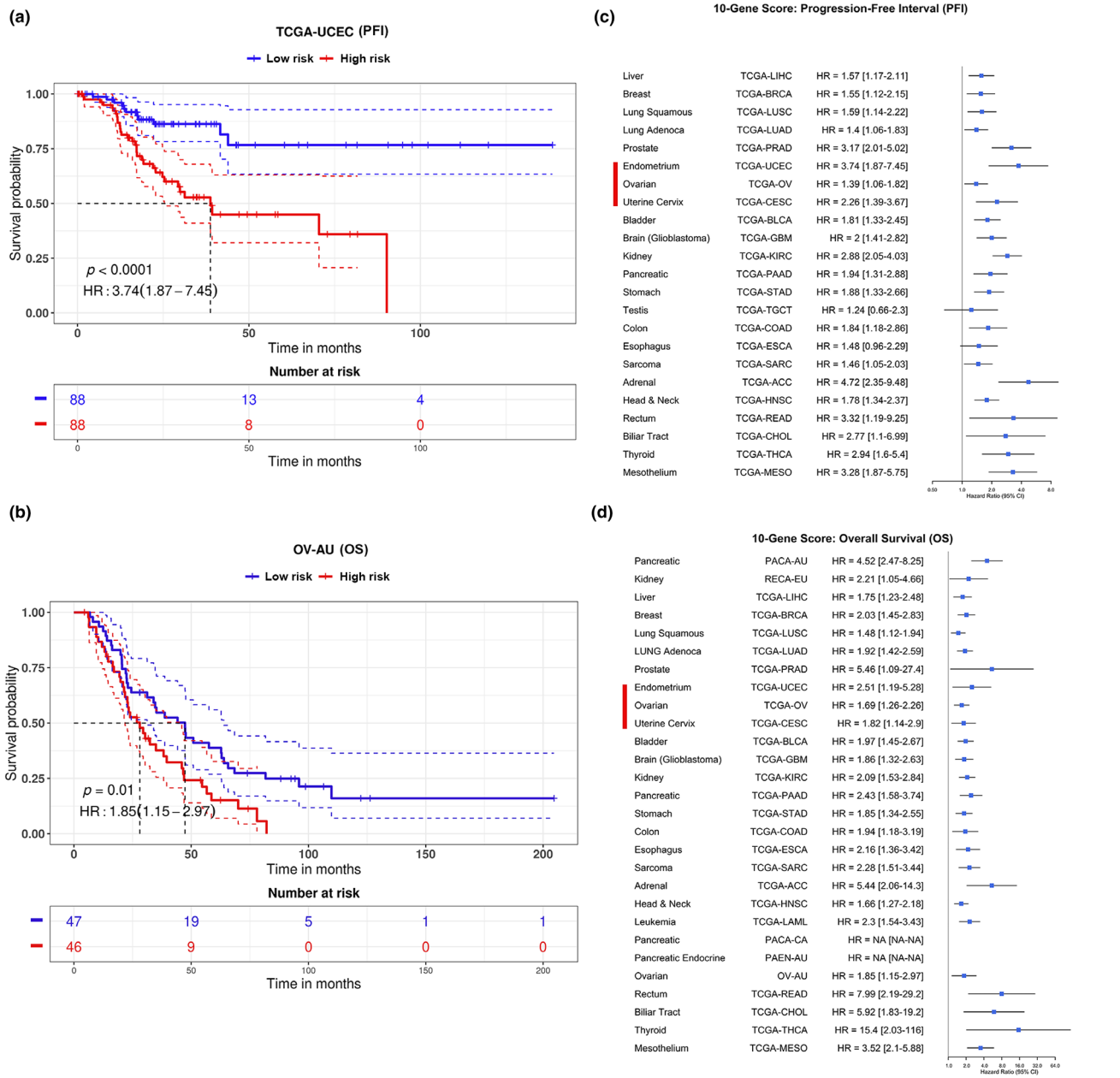

FIGURE 2 Validation of the 10-gene score across cancer types and endpoints. (a, b) Kaplan–Meier curves for progression-free interval (UCEC-TCGA) and overall survival (OV-AU) stratified by risk group. (c, d) Forest plots from multivariable Cox models across 23 (PFI) and 28 (OS) cohorts. Abbreviations: OS, overall survival; PFI, progression-free interval; UCEC, uterine corpus endometrial carcinoma; OV-AU, ovarian cancer (Australian cohort).

Even using unweighted scores from ToPP,[27] the panel retained strong performance (Figure 2e).

The final panel included *ABCA13*, *ADAM15*, *ANO4*, *B4GALNT1*, *CGB8*, *COL11A1*, *EIF3J*, *IGF2BP2*, *SAMD9*, and *TERT*. The functional annotations, direction of effect, and novelty index for each of the 10 genes are summarized in Table S5.

To ensure compatibility with FFPE-based assays, a nine-gene version (excluding *CGB8*, a placental gene inconsistently detected in spatial data) was also validated, showing equivalent performance (Figure S1).

3.3 | Internal validation and multivariable modeling

In pooled TCGA pan-cancer data, the score stratified risk for OS and PFI (Figure 3a,b). Multivariable Cox models adjusting for tumor type and clinical, and demographic variables confirmed independent prognostic value (hazard ratio [HR] = 2.15 [1.60–2.88], $P < 0.001$).

Bootstrap simulations (1000 iterations) demonstrated coefficient stability (Figure 3c,d). The FFPE-adapted score showed similar results (Figure S1), confirming cross-platform robustness.

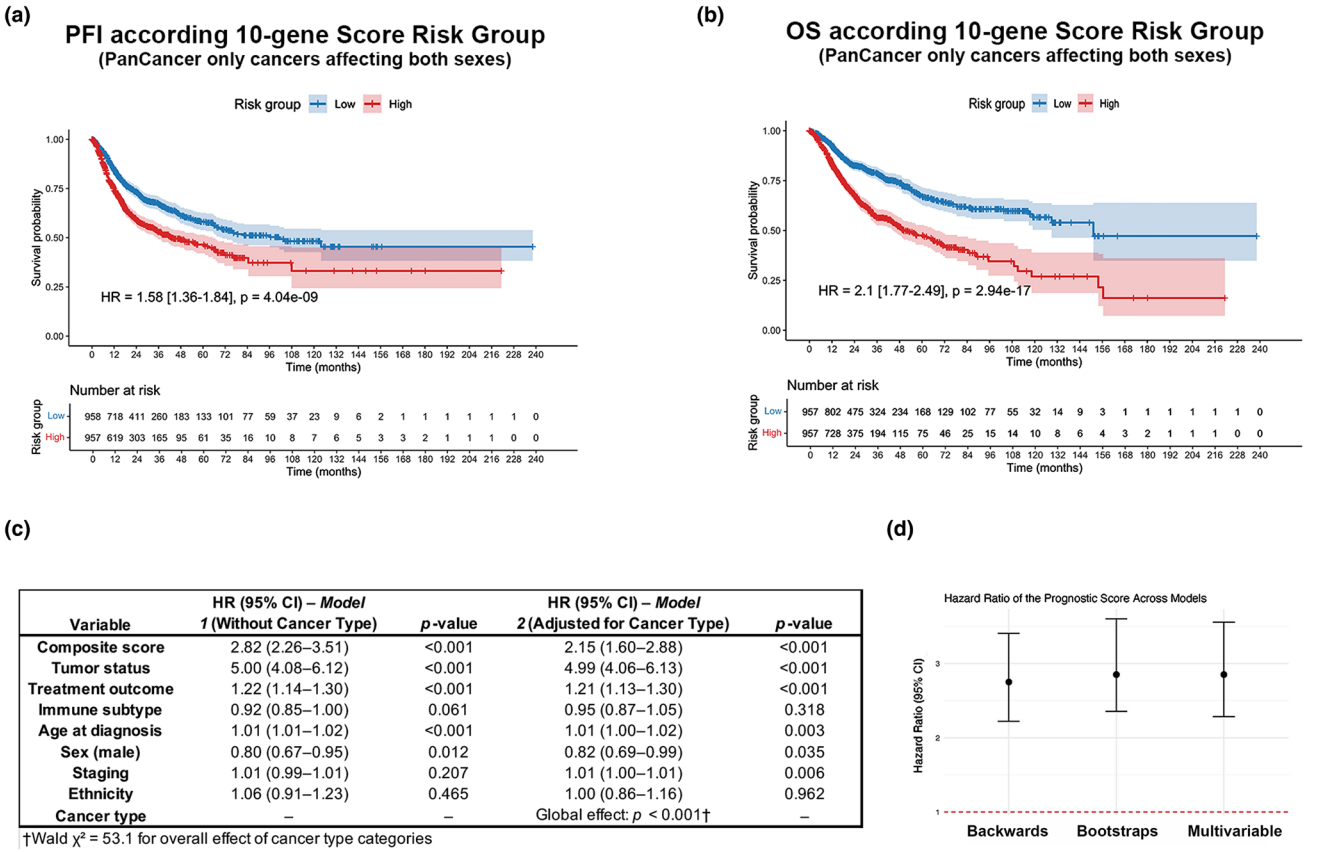

(c)

Variable	HR (95% CI) – *Model 1* (Without Cancer Type)	*p*-value	HR (95% CI) – *Model 2* (Adjusted for Cancer Type)	*p*-value
Composite score	2.82 (2.26–3.51)	<0.001	2.15 (1.60–2.88)	<0.001
Tumor status	5.00 (4.08–6.12)	<0.001	4.99 (4.06–6.13)	<0.001
Treatment outcome	1.22 (1.14–1.30)	<0.001	1.21 (1.13–1.30)	<0.001
Immune subtype	0.92 (0.85–1.00)	0.061	0.95 (0.87–1.05)	0.318
Age at diagnosis	1.01 (1.01–1.02)	<0.001	1.01 (1.00–1.02)	0.003
Sex (male)	0.80 (0.67–0.95)	0.012	0.82 (0.69–0.99)	0.035
Staging	1.01 (0.99–1.01)	0.207	1.01 (1.00–1.01)	0.006
Ethnicity	1.06 (0.91–1.23)	0.465	1.00 (0.86–1.16)	0.962
Cancer type	–	–	Global effect: $p < 0.001$†	–

†Wald $\chi^2 = 53.1$ for overall effect of cancer type categories

(d)

FIGURE 3 Multivariable performance and robustness of the score. (a, b) Pooled Kaplan–Meier survival analysis for OS and PFI across all cancers. (c) Multivariable Cox model adjusting for tumor type, stage, and clinical variables. (d) Bootstrap-derived stability of coefficients over 1000 iterations. Abbreviations: OS, overall survival; PFI, progression-free interval.

3.4 | Clinical utility and prognostic stratification across cohorts

Time-dependent areas under the curve (AUCs) and calibration slopes were estimated with 1000 bootstrap resamples to derive 95% confidence intervals (CIs). Calibration intercepts and slopes were assessed with bootstrap-corrected 95% CIs. Time-dependent ROC curves showed AUCs of 0.69 (95% CI 0.66–0.72), 0.71 (0.68–0.74), and 0.72 (0.69–0.75) at 1, 3, and 5 years, respectively (Figure 4a). Calibration plots demonstrated good agreement between predicted and observed outcomes at 3 years (Figure 4b).

We developed a multivariable prognostic nomogram integrating tumor type, stage, immune subtype, and treatment response, which retained strong discrimination and calibration (Figure 4c). Across all cohorts, 95% CIs for time-dependent AUCs overlapped between datasets, supporting model stability and calibration consistency (AUC range 0.69–0.72).

3.5 | External validation in CPTAC proteogenomic cohorts

We validated the score in the CPTAC-3 proteogenomic dataset ($n = 2191$) across 10 tumors. Kaplan–Meier analyses confirmed clear stratification (HR = 2.21, $P < 0.0001$; Figure 5a). Although multivariable-adjusted models showed reduced significance (HR = 1.12, $P = 0.275$; Figure 5b), the overall trends remained consistent. The attenuation of adjusted hazard ratios in CPTAC (adjusted HR 1.12, $P = 0.275$) likely reflects differences in cohort composition, reduced availability of microenvironmental covariates, and the proteomic nature of CPTAC data, which are less sensitive to stromal or immune programs captured at the transcriptomic level. Despite this, discrimination (AUC range 0.68–0.72, 95% CI 0.65–0.74) and calibration remained acceptable (Figure 5c), indicating that transcriptomic risk signals are retained across platforms but require prospective validation for clinical deployment.

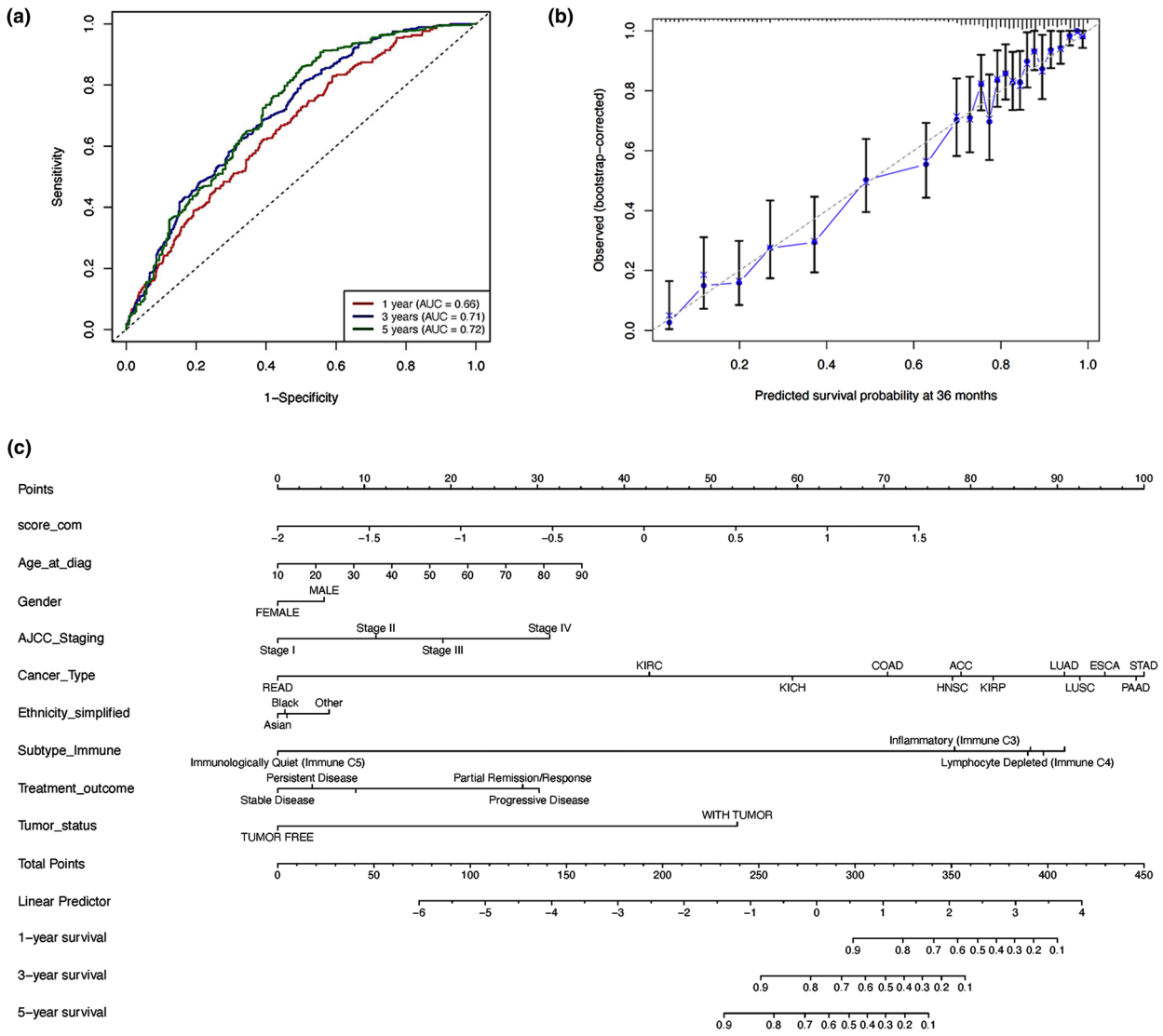

FIGURE 4 Clinical risk prediction and nomogram development. (a) Time-dependent receiver operating characteristic (ROC) analysis of the 10-gene score at 1, 3, and 5 years. (b) Calibration plot at 3 years comparing predicted versus observed survival. (c) Prognostic nomogram integrating score with tumor type, immune subtype, stage, and treatment outcome. Abbreviations: ROC, receiver operating characteristic; AUC, area under the curve; CI, confidence interval.

3.6 | Decision curve analysis and clinical net benefit

Continuous and binary versions of the score were compared using ROC and DCA. The continuous score provided higher net benefit for residual disease and treatment outcomes (Figure S2).

Net reclassification improvement (NRI = +0.29) indicated enhanced patient stratification.

3.7 | Multi-level biological insights: Bulk, single-cell, and spatial analyses

Gene set enrichment analysis (GSEA) revealed enrichment of inflammatory, EMT, and immune exhaustion pathways in high-score tumors (Figure 6a–c).

EcoTyper analysis confirmed immunosuppressive ecotypes in high-score groups across multiple cancers, including gynecologic (Figure 6d; Figure S3A; Table S5).

We analyzed 33 single-cell RNA-seq samples (cervical, endometrial, and ovarian tumors) using two scores per cell:

- *10-gene score*: the prognostic model, computed as the mean normalized expression of the 10 genes.
- *ICI score*: mean scaled expression of *CD274 (PD-L1)*, *PDCD1 (PD-1)*, *CTLA4*, *LAG3*, *HAVCR2 (TIM-3)*, and *TIGIT*.

Violin plots showed the 10-gene score enriched in malignant cells and fibroblasts, while the ICI score was highest in $CD8^+$ T cells, NK cells, and macrophages (Figure 6e).

Correlation analysis showed moderate association between scores in $CD8^+$ T and NK cells, and minimal correlation in fibroblasts and

(a)

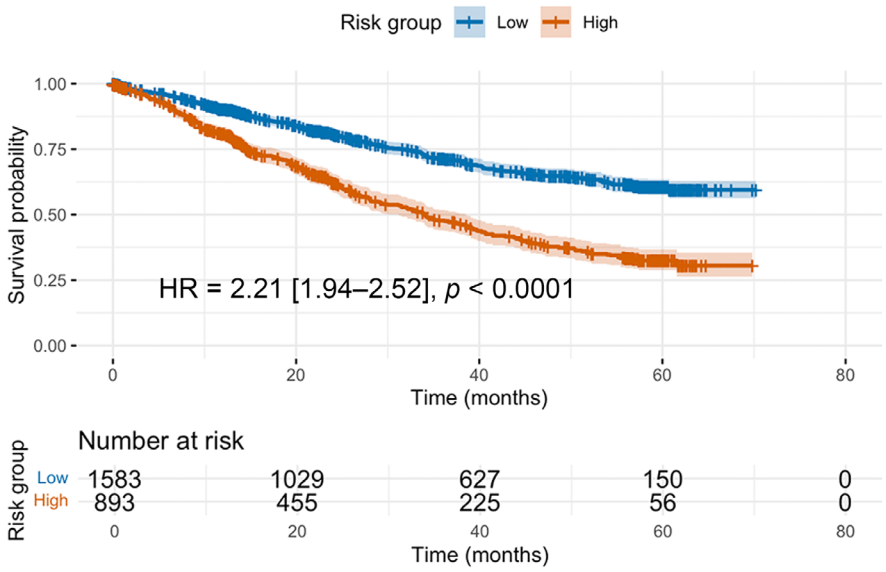

(b)

Variable	HR (95% CI) – Model 1 (Unadjusted for tumor type)	*p*-value	HR (95% CI) – Model 2 (Adjusted for tumor type)	*p*-value
Composite score	1.88 (1.59–2.22)	<0.001	1.12 (0.91–1.38)	0.275
Tumor status – R1	2.23 (1.76–2.83)	<0.001	1.52 (1.18–1.96)	0.001
Tumor status – R2	3.23 (1.78–5.86)	<0.001	1.90 (1.02–3.52)	0.043
Tumor status – RX	0.88 (0.72–1.07)	0.184	0.90 (0.74–1.10)	0.316
Stage – IA	0.21 (0.05–0.87)	0.032	0.20 (0.05–0.84)	0.028
Stage – I	0.13 (0.03–0.53)	0.004	0.17 (0.04–0.74)	0.018
Sex – male	1.03 (0.87–1.20)	0.758	1.04 (0.87–1.25)	0.633
Tumor type (global)	–	–	$p < 0.001$†	–

† Wald $\chi^2 = 595$ on 36 df, $p < 0.001$ for the overall effect of tumor type.

(c)

Metric	PanCancer	CPTAC-3
HR (score) – unadjusted	2.82 (2.26–3.51)	1.88 (1.59–2.22)
p-value (unadjusted)	<0.001	<0.001
HR (score) – adjusted for tumor type	2.15 (1.60–2.88)	1.12 (0.91–1.38)
p-value (adjusted)	<0.001	0.275
Concordance – unadjusted	0.739	0.739
Concordance – adjusted	0.766	0.766
N patients	1915	2191
Global p (tumor type)	<0.001 ($\chi^2 = 53.1$, df=11)	<0.001 ($\chi^2 = 595$, df=36)

FIGURE 5 External validation in proteogenomic data. (a) Kaplan–Meier curve for the CPTAC-3 cohort ($n = 2191$) using dichotomized risk groups. (b) Multivariable Cox model adjusted for clinical variables. (c) Comparative metrics between TCGA and CPTAC datasets confirm cross-platform robustness. Abbreviations: CPTAC, Clinical Proteomic Tumor Analysis Consortium; TCGA, The Cancer Genome Atlas; AUC, area under the curve.

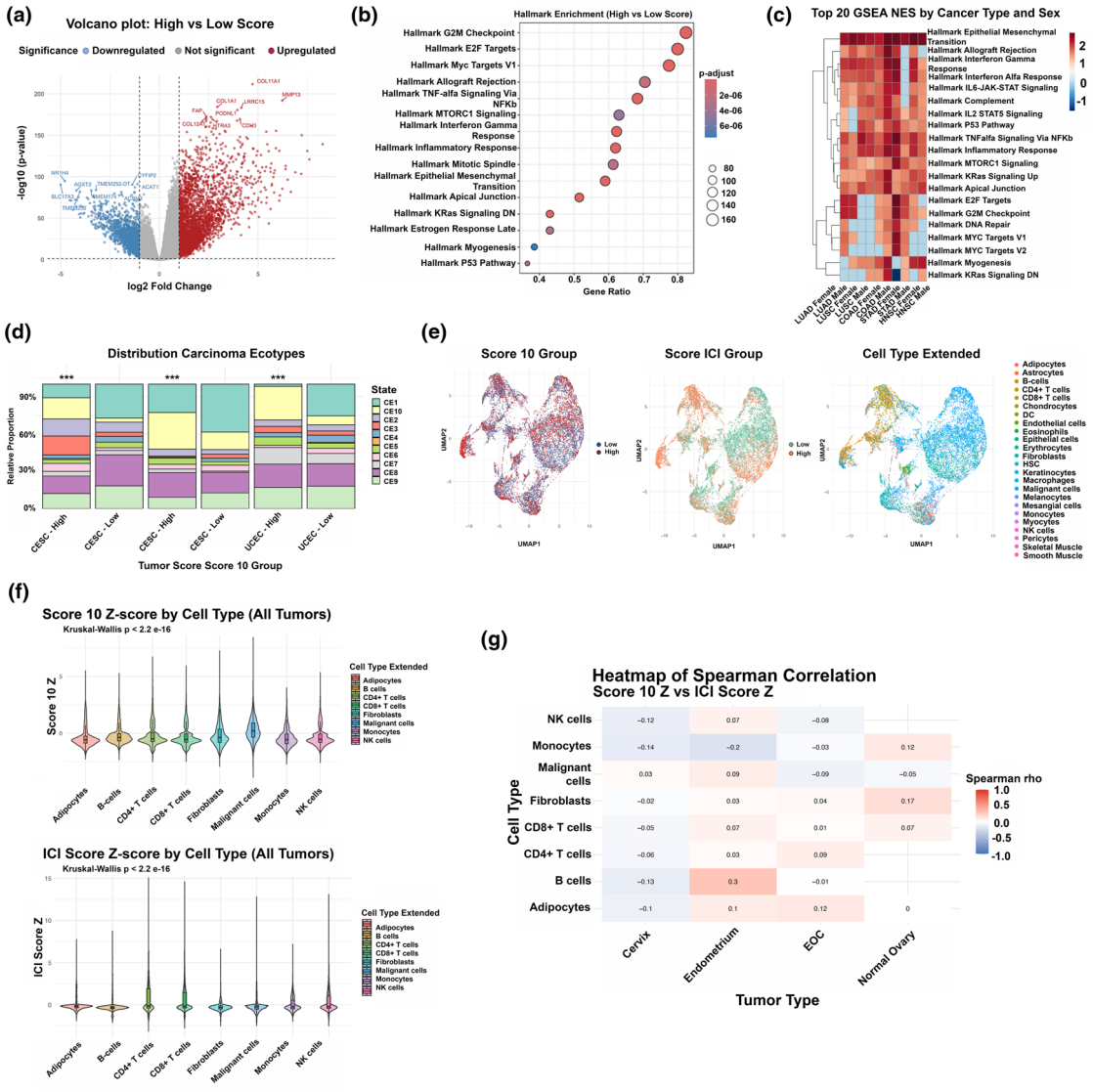

FIGURE 6 Multi-level biological and single-cell analysis of the 10-gene sex-informed prognostic score across gynecologic cancers. (a) Volcano plot displaying differentially expressed genes between high- and low-score tumors. Significantly upregulated genes (red) include extracellular-matrix and immunosuppressive mediators, whereas downregulated genes (blue) are enriched for immune-activation signatures. (b) Hallmark pathway enrichment analysis (GSEA) of high- versus low-score tumors identifies suppression of immune and interferon responses and activation of matrix- and TGF-β-related pathways. (c) Heatmap showing the top 20 GSEA normalized enrichment scores (NES) across cancer types and sexes, highlighting consistent enrichment of epithelial–mesenchymal transition (EMT), TGF-β signaling, and hypoxia programs in high-score tumors. (d) Distribution of carcinoma ecotypes (C01–C09) according to Score 10 group across cervical (CESC), endometrial (UCEC), and ovarian (OV) cancers, demonstrating higher prevalence of stromal/immunosuppressive ecotypes (C04, C06) in high-score tumors (χ^2 test, *** ($P < 0.001$)). (e) UMAP projections of integrated single-cell datasets ($n > 150{,}000$ cells) showing cell clustering by 10-gene score group, by ICI score group, and by extended cell-type annotation (malignant, fibroblast, endothelial, immune subsets). (f) Violin plots displaying standardized Z-scores of the 10-gene score and ICIscore1 across all cell types. The 10-gene score is highest in malignant and fibroblast cells, whereas ICIscore1 is enriched in $CD8^+$ T and NK cells (Kruskal–Wallis, ($P < 0.001$)). (g) Heatmap of Spearman correlations between Score 10 Z and ICIscore1 Z per cell type and tumor type, showing positive correlations in cytotoxic lymphocytes and minimal association in stromal compartments. Abbreviations: GSEA, gene set enrichment analysis; NES, normalized enrichment score; EMT, epithelial–mesenchymal transition; TGF-β, transforming growth factor beta; ICI, immune checkpoint inhibitor; NK, natural killer; UMAP, uniform manifold approximation and projection.

monocytes (Figure 6f), indicating distinct yet partially overlapping axes of immune activity and tumor aggressiveness.

Cervical tumors exhibited the highest ICI scores, followed by endometrial, while ovarian tumors showed more immune-excluded profiles. These differences might help explain variable immunotherapy responses in gynecologic cancers.

3.8 | Spatial transcriptomic findings

Spatial data from ovarian, cervical, prostate, and colorectal tumors profiled via 10× Visium confirmed that high-score regions aligned with malignant epithelial zones and fibroblast-rich areas, while low-score regions showed higher $CD4^+$ and $CD8^+$ T cell presence (Figures 7a–c and 8a–c; Figures S5a–c and S6a–c).

Checkpoint analysis showed significantly higher *PDCD1* and *CTLA4* expression in high-score colorectal regions ($P < 0.01$) but no differences in *CD274* across tumor types (Figures 7d and 8d; Figures S5d and S6d).

These spatial patterns, particularly robust in cervical and ovarian tumors, support the model's relevance in identifying immune-excluded, high-risk microenvironments.

3.9 | Gene dependency and novelty across oncogenic databases

CRISPR-Cas9 dependency data (DepMap 24Q4[37]) showed no significant CERES-based dependency for the 10 genes across approximately 700 cell lines (Figure S7), suggesting that the score reflects systems-level aggressiveness rather than single-gene essentiality.

Annotation using OncoKB, COSMIC, MSK-IMPACT, FoundationOne, Vogelstein's list, and OncoMD[22,38–42] confirmed limited overlap with canonical oncogenes (Figure S8).

A composite novelty index (0–6) confirmed the distinctiveness of this signature.

3.10 | Integrated summary of biological and clinical findings

This integrative analysis confirms that the 10-gene score identifies tumors with conserved transcriptional programs of aggressiveness, stromal remodeling, and immune evasion. Its reproducibility across platforms, including single-cell and spatial resolution, supports its potential as a robust tool for risk stratification, with immediate applicability in gynecologic oncology.

4 | DISCUSSION

Understanding the transcriptional programs underlying tumor aggressiveness remains a central challenge in precision oncology. Here, we developed and validated a sex-informed 10-gene prognostic score using large-scale, publicly available datasets. Although sex was explicitly considered during the discovery phase, the final 10-gene score does not include sex as an input variable. The resulting model is, therefore, sex-agnostic (applicable to both sexes) while preserving the biological insights derived from sex-aware analyses. The score provides a biologically grounded framework to assess immune escape and tumor aggressiveness, although it is not yet ready for routine clinical use.

Consistent results across 28 TCGA tumor types were validated using independent proteogenomic (CPTAC), single-cell, and spatial transcriptomic data. This confirms the power of open-access repositories to identify reproducible transcriptomic correlates of prognosis and immune evasion.[3,27,43] Nonetheless, the reliance on public datasets (largely derived from high-income countries and populations of European ancestry) might limit generalizability across ethnically and geographically diverse patient groups.[44,45] This limitation underscores the urgent need for more diverse transcriptomic datasets representative of low- and middle-income countries.

Unlike earlier approaches limited to bulk RNA-seq or single-cohort derivation, this model integrates immune deconvolution, spatial architecture, and CRISPR functional data, reinforcing its translational relevance. Detailed annotation and functional categorization of the 10 genes included in the prognostic score are provided in Table S5.

Compared with established molecular classifiers—such as the TCGA molecular taxonomy of endometrial carcinoma,[46] the ProMisE (Proactive Molecular Risk Classifier for Endometrial Cancer) system,[47] and the molecularly integrated TransPORTEC model for endometrial cancer[48]—our 10-gene score provides a compact, transcriptomic-only metric that captures immune and stromal programs often missed by mutational or histopathologic subtyping. In ovarian cancer, the score differs from transcriptomic classifiers derived from TCGA and the Tothill subtypes[49] or the Verhaak refinement,[50] which mainly describe tumor-intrinsic lineages rather than immune-exclusion states. Similarly, in cervical cancer, it extends beyond the TCGA integrated genomic classification[51] by incorporating immune and stromal signatures associated with checkpoint resistance. Together, these comparisons highlight the complementary role of this model within existing molecular stratification frameworks across gynecologic malignancies.

The score reflects a conserved transcriptional program involving inflammation, stromal remodeling, and immune suppression. GSEA across TCGA tumors revealed upregulation of *IFN-γ*, *IL6–JAK–STAT3*, and EMT signaling in high-score tumors (Figure 6a–c). Using EcoTyper,[36] we confirmed the enrichment of immunosuppressive ecotypes in high-score tumors, including those of gynecologic origin (Figure 6d; Figures S3A).

In 33 single-cell datasets from ovarian, endometrial, and cervical tumors, the 10-gene score was enriched in malignant epithelial cells and fibroblasts and absent in normal compartments. Conversely, the *ICI score*, based on *PDCD1*, *CTLA4*, *CD274*, *LAG3*, *HAVCR2*, and *TIGIT*, was elevated in $CD8^+/CD4^+$ T cells and NK cells. UMAP and violin plots revealed that cervical and endometrial tumors had higher

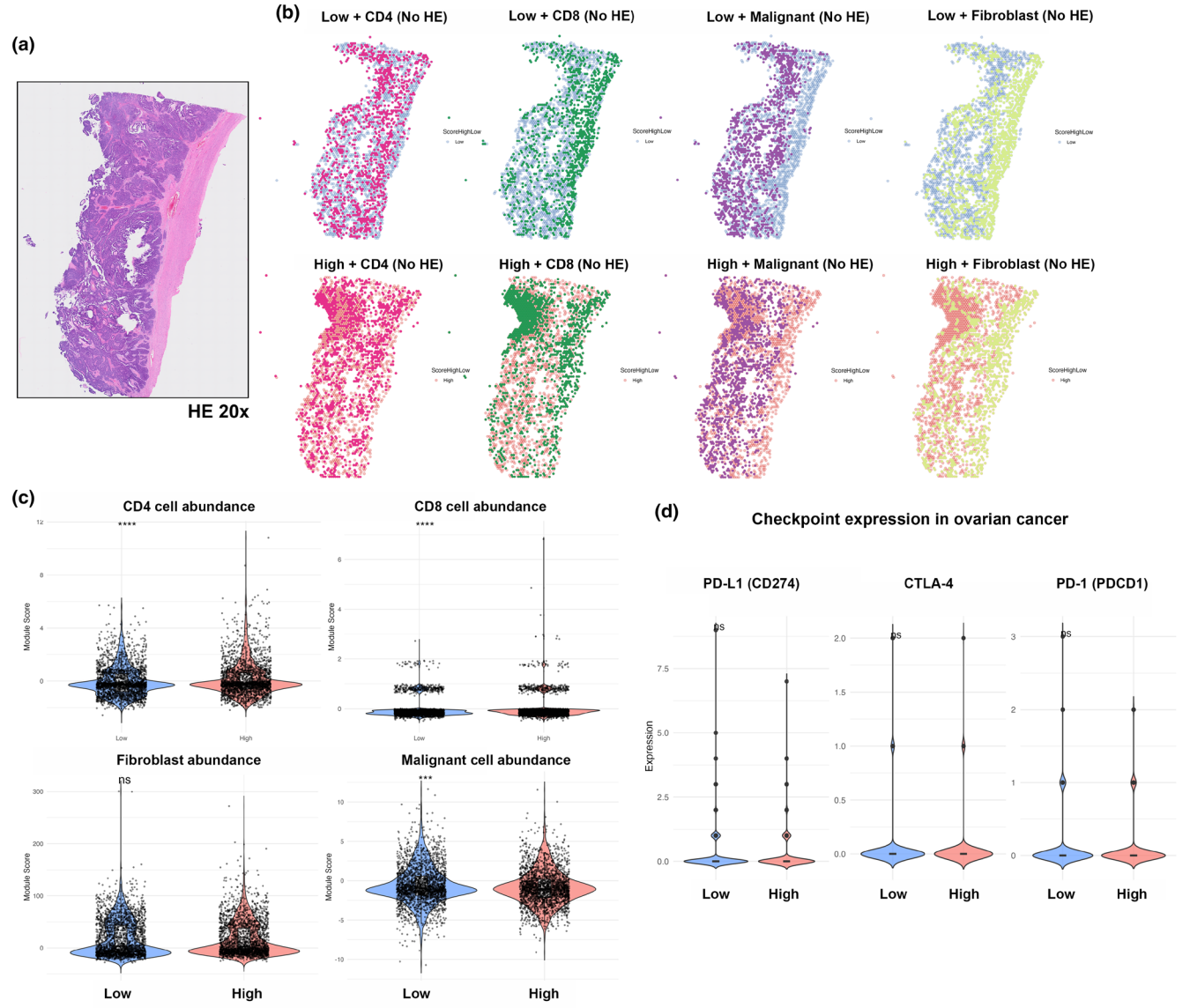

FIGURE 7 Spatial and molecular characterization of the prognostic score in ovarian cancer. (a) Hematoxylin and eosin (H&E) image of an FFPE ovarian tumor section profiled using 10x Genomics Visium. (b) Spatial maps displaying the distribution of $CD4^+$ and $CD8^+$ T cells, malignant epithelial cells, and fibroblasts across low-score (top row) and high-score (bottom row) regions. High-score areas show clear immune exclusion (reduced $CD4^+$ and $CD8^+$ T cells) and stromal/malignant enrichment. (c) Violin plots comparing cell-type abundance between score-defined regions. (d) Expression of immune checkpoints PD-L1 (CD274), CTLA-4, and PD-1 (PDCD1) by score group in ovarian cancer. Abbreviations: H&E, hematoxylin and eosin; FFPE, formalin-fixed paraffin-embedded; PD-L1, programmed death-ligand 1; PD-1, programmed cell death 1; CTLA-4, cytotoxic T-lymphocyte–associated protein 4.

Score10 expression in malignant cells compared to ovarian tumors, while the *ICI score* showed the highest values in cervical tumors (Figure 6e–g). Their moderate correlation in $CD8^+$ and NK cells and minimal overlap in stromal and myeloid compartments, suggests distinct but partially convergent biological axes (Figure 6f). These cell-type-specific differences not only inform tumor biology but also highlight opportunities to therapeutically target the immunosuppressive niche, such as reprogramming fibroblasts or restoring cytotoxic infiltration.

Spatial transcriptomics reinforced these insights. In ovarian and cervical tumors, high-score regions aligned with malignant/fibroblast-dense areas, whereas low-score regions had increased $CD4^+$ and $CD8^+$ T cell infiltration. These patterns were less clear in prostate and colorectal tumors (Figures 7a–c and 8a–c; Figures S5a–c and S6a–c). While *PDCD1* and *CTLA4* were elevated in high-score regions of colorectal tumors, *CD274* did not differ across score groups or tumor types (Figures 7d and 8d; Figures S5d and S6d). These findings support the presence of conserved immune exclusion patterns, particularly in gynecologic malignancies. Such patterns might underlie the limited efficacy of immunotherapies in tumors with fibrotic or immunosuppressed microenvironments and support the rationale for combinatorial strategies.

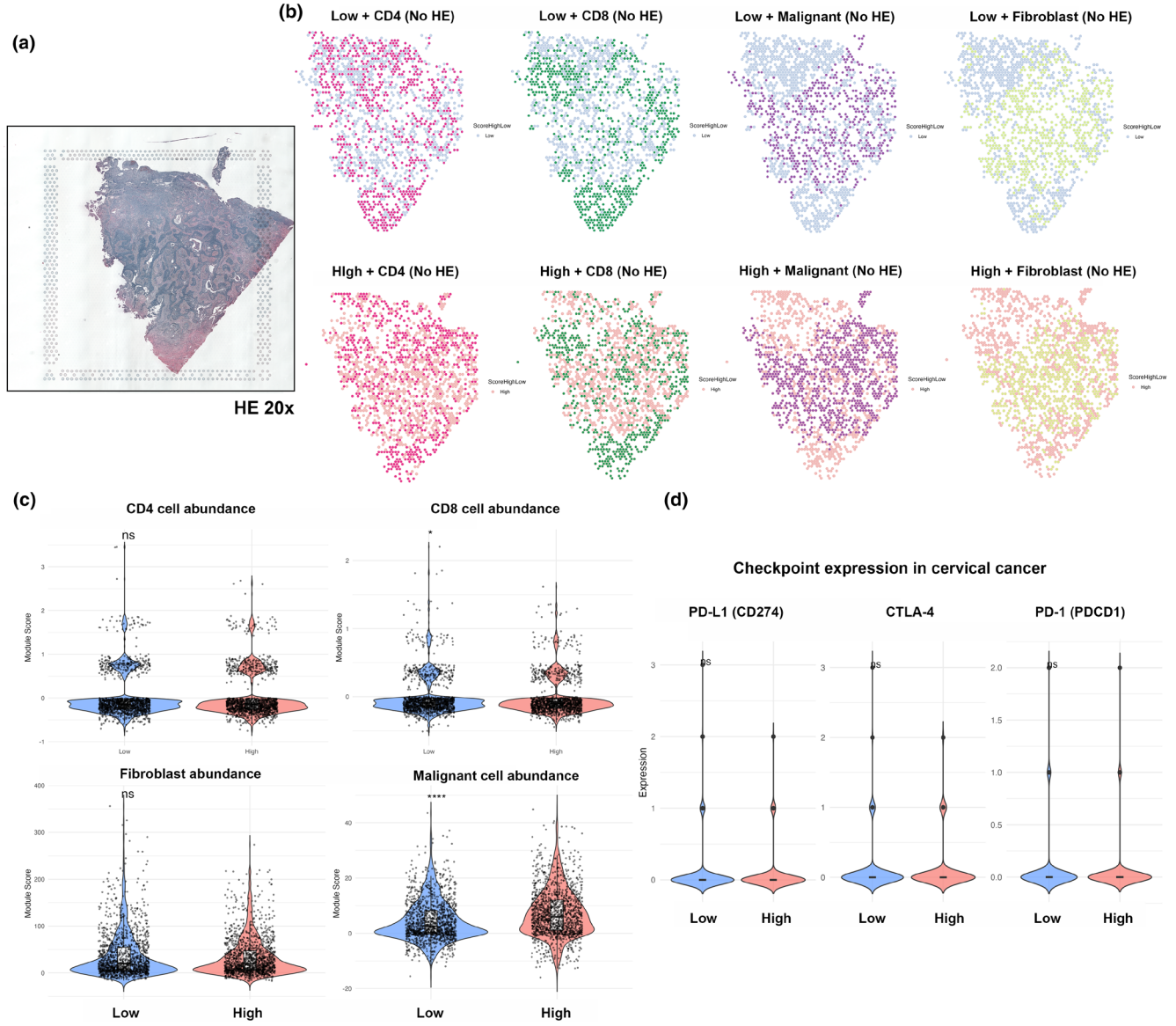

FIGURE 8 Spatial and molecular characterization of the prognostic score in cervical cancer. (a) Representative H&E image (20×) of an FFPE cervical tumor section profiled using 10x Genomics Visium spatial transcriptomics. (b) Spatial distribution of $CD4^+$ and $CD8^+$ T cells, malignant epithelial cells, and fibroblasts across score-defined regions (Low vs. High). (c) Violin plots comparing cell-type abundance between low- and high-score regions. (d) Expression of immune checkpoints PD-L1 (CD274), CTLA-4, and PD-1 (PDCD1) stratified by score group in cervical cancer. Abbreviations: H&E, hematoxylin and eosin; FFPE, formalin-fixed paraffin-embedded; PD-L1, programmed death-ligand 1; PD-1, programmed cell death 1; CTLA-4, cytotoxic T-lymphocyte–associated protein 4.

These findings are consistent with a mechanistic model in which cancer-associated fibroblasts and extracellular-matrix remodeling, driven by TGF-β and IL6–JAK–STAT3 signaling, create physical and cytokine barriers to cytotoxic T-cell infiltration, leading to immune-excluded niches and checkpoint resistance. Figure 9 illustrates this proposed pathway linking stromal remodeling to immune evasion.

This has clinical implications. In ovarian and cervical cancers, where PD-L1 expression often fails to predict response, our score identifies tumors with transcriptional aggressiveness and immunosuppressive niches, even in PD-L1–negative settings.[52–55] This supports its potential role in guiding combinatorial strategies, such as immune checkpoint blockade combined with anti-fibrotic agents or IL6–JAK inhibitors, especially in tumors lacking classical predictive markers. The biological link between transcriptomic risk and immune resistance likely reflects stromal remodeling and cytokine-driven immune exclusion. High-score tumors exhibit activation of fibroblast and extracellular-matrix programs (mediated by *COL11A1*, *ADAM15*, and related genes) together with cytokine signaling through *IL6–JAK–STAT3* and *TGF-β* pathways. These processes generate a fibroblast-rich stromal barrier that limits $CD8^+$ T-cell infiltration and promotes T-cell exhaustion, thereby explaining PD-L1–independent immune evasion observed in these tumors. This integrative model (Figure 9) summarizes the proposed mechanistic cascade linking stromal

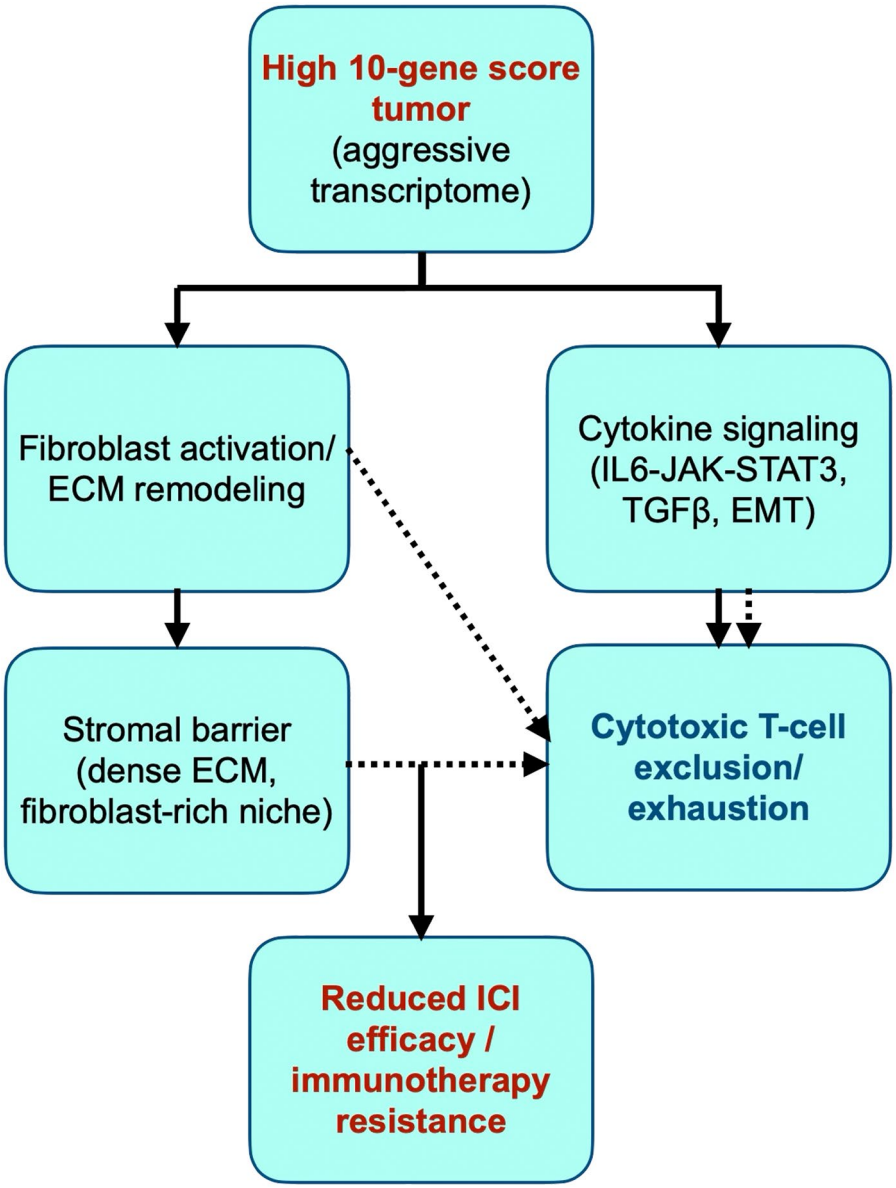

FIGURE 9 Conceptual model linking transcriptomic risk, stromal remodeling, and immune exclusion in high-score tumors. High 10-gene transcriptomic scores are associated with fibroblast activation, extracellular matrix (ECM) remodeling, and immunosuppressive cytokine signaling, which collectively promote immune exclusion and reduced efficacy of immune-checkpoint inhibitors (ICIs). Upregulation of genes such as *COL11A1* and ADAM15 reflects fibroblast activation and matrix deposition, whereas activation of *IL6–JAK–STAT3* and *TGF-β* pathways promotes cytokine-driven epithelial–mesenchymal transition (EMT) and T-cell dysfunction. These processes generate a fibroblast-rich stromal barrier that limits $CD8^+$ T-cell infiltration and promotes T-cell exhaustion, ultimately leading to checkpoint-therapy resistance. Abbreviations: ECM, extracellular matrix; EMT, epithelial–mesenchymal transition; ICI, immune checkpoint inhibitor; JAK, Janus kinase; STAT3, signal transducer and activator of transcription 3; TGF-β, transforming growth factor beta.

remodeling to immune exclusion and reduced response to immune-checkpoint inhibitors, supported by recent spatial-transcriptomic and experimental studies.[56–58] The presence of immunosuppressive programs and fibroblast-rich niches, independent of PD-L1 expression, might explain immune exclusion in these tumors.

External validation in CPTAC ($n=2191$, across 10 tumor types) confirmed strong risk stratification (HR = 2.21, $P<0.0001$), despite attenuation in adjusted models (HR = 1.12, $P=0.275$), likely due to limited transcriptomic or immune-deconvolution variables in CPTAC datasets, which focus primarily on proteomic and mutational data rather than microenvironmental features (Figure 5a–c). These results emphasize robustness across platforms and highlight the utility of transcriptomic biomarkers beyond TCGA.[23]

From a clinical utility perspective, time-dependent ROC curves, calibration plots, and DCA confirmed stable performance (Figure 4a–c). The continuous version outperformed binary classification and yielded a net reclassification improvement (NRI = +0.29), highlighting the importance of preserving continuous information.[32,33] For clinical translation, the score can be reported as a continuous variable or dichotomized at the cohort median for pragmatic risk grouping.

Decision-curve analysis favored the continuous formulation, but a median or tertile cut-off could be adopted for trial stratification or adjuvant-risk discussions. For instance, in a hypothetical clinical scenario, patients with high transcriptomic risk but PD-L1–negative tumors could be prioritized for combinatorial regimens (e.g., checkpoint blockade + anti-fibrotic therapy), while low-risk cases might safely receive single-agent immunotherapy. In gynecologic oncology, the score could complement established classifiers such as ProMisE and TCGA molecular subtypes by identifying immune-excluded or fibroblast-rich phenotypes in PD-L1–negative tumors where checkpoint monotherapy is less effective. With only 10 genes, the model could be implemented via NanoString, RT-qPCR, or targeted sequencing, enabling use in FFPE samples and standard pathology workflows. This simplicity facilitates implementation in adaptive clinical trials or decentralized settings, where streamlined molecular assays are needed. However, clinical thresholds and therapeutic algorithms still require prospective validation before routine deployment.

Importantly, no individual gene showed significant CRISPR-based dependency in CERES data from DepMap 24Q4[37] (Figure S7), indicating that the score captures systems-level states (emergent phenotypes shaped by network-level reprogramming) rather than isolated oncogenic drivers.

Annotation using OncoKB,[38] COSMIC,[39] MSK-IMPACT,[22] FoundationOne,[40] Vogelstein's list,[41] and OncoMD[42] revealed that only *TERT* and *SAMD9* were previously catalogued as oncogenes. Mutation-expression analyses using OncoMD showed no expression differences by mutational status, confirming the score reflects transcriptional reprogramming rather than mutation-driven phenotypes.[59] Additionally, *IGF2BP2* has been recognized as a key post-transcriptional regulator via m6A RNA methylation reading, contributing to oncogenic plasticity in the absence of genetic alterations.[60]

This work is inherently limited by its retrospective design and reliance on publicly available datasets largely derived from high-income populations, underscoring the need for more diverse transcriptomic resources encompassing low- and middle-income settings.

5 | FUTURE DIRECTIONS AND TRANSLATIONAL POTENTIAL

While not yet ready for clinical application, this model offers several paths forward. Its continuous form facilitates use in prognostic models and clinical trials, particularly where PD-L1 or TMB fail to predict response. Its structure is compatible with FFPE-based platforms, and simplified assays might allow implementation in low-resource settings, contributing to equity in precision oncology.

Biologically, the score captures features often overlooked in genomics: immune exclusion, fibroblast activation, and stromal remodeling. In tumors like ovarian and cervical cancer, where checkpoint inhibitors show inconsistent efficacy, this model might help define “immune-cold” phenotypes and guide personalized treatment strategies.

Randomized prospective validation, ideally in biomarker-driven trials, is essential. In such settings, the score might serve as a stratification biomarker to identify patients less likely to respond to monotherapy and more likely to benefit from combined immune-modulating regimens. We propose testing the score in gynecologic oncology as a high-impact setting. Mechanistic studies on the lesser-known genes included in the score could yield therapeutic insights, particularly through integration with proteomic, spatial, and epigenetic data. Moreover, its application in longitudinal studies might help evaluate treatment-induced microenvironmental shifts and inform response-adapted strategies.

In summary, this 10-gene sex-informed prognostic score captures high-risk transcriptional states across tumor types, including gynecologic malignancies. It represents a scalable model for future biomarker development, integrating multi-platform validation with clinical and biological insight. Its inclusion in stratified trial designs could accelerate precision oncology beyond current PD-L1–dependent frameworks.

AUTHOR CONTRIBUTIONS

MAC conceived and supervised the study. MAC, FGV, and IW developed the methodology. FGV and IW acquired and curated the data. MAC, FGV, and IW performed the statistical and transcriptomic analyses. SK and CI contributed to technical and material support and critically reviewed the manuscript. All authors (MAC, FGV, IW, SK, and CI) revised and approved the final version of the manuscript and meet ICMJE criteria for authorship.

ACKNOWLEDGMENTS

The authors acknowledge the use of publicly available datasets from TCGA, UCSC Xena, MSK-IMPACT, CPTAC, and GEO. AI-based tools (e.g., ChatGPT) were used to assist with English language editing and literature search. Their use was limited to improving clarity and presentation under full human oversight and verification.

FUNDING INFORMATION

This study was supported by the Chilean National Research Center on Advanced Frontal Development (FONDAP 152220002).

CONFLICT OF INTEREST STATEMENT

The authors declare no potential conflicts of interest.

DATA AVAILABILITY STATEMENT

All datasets used in this study are publicly available. Gene expression and clinical data were retrieved from UCSC Xena (https://xenabrowser.net), cBioPortal (https://www.cbioportal.org), and 10× Genomics (https://www.10xgenomics.com). Proteogenomic data generated by the Clinical Proteomic Tumor Analysis Consortium (CPTAC) were accessed through the NIH dbGaP portal (accession number: phs001287.v5.p4), in accordance with data use agreements. Data were retrieved in June 2025. The datasets analyzed during the current study are available from the corresponding author upon reasonable request. All scripts used for score construction, gene

weights, and analytic pipelines are openly available at: https://github.com/macuello1968/sex-informed-score.

ETHICS STATEMENT

All datasets analyzed were previously collected under IRB-approved protocols and informed consent as part of their original studies. No additional ethics approval was required for this secondary analysis.

CONSENT

Not applicable.

ORCID

Mauricio A. Cuello https://orcid.org/0000-0003-2812-0015
Fernán Gómez-Valenzuela https://orcid.org/0000-0001-6889-976X
Ignacio Wichmann https://orcid.org/0000-0002-1115-2937

REFERENCES

1. Bray F, Laversanne M, Sung H, et al. Global cancer statistics 2022: GLOBOCAN estimates of incidence and mortality worldwide for 36 cancers in 185 countries. *CA Cancer J Clin*. 2024;74(3):229-263.
2. Cook MB, McGlynn KA, Devesa SS, Freedman ND, Anderson WF. Sex disparities in cancer mortality and survival. *Cancer Epidemiol Biomarkers Prev*. 2011;20(8):1629-1637.
3. Kim HI, Lim H, Moon A. Sex differences in cancer: epidemiology, genetics and therapy. *Biomol Ther Seoul*. 2018;26(4):335-342.
4. Li CH, Haider S, Shiah YJ, Thai K, Boutros PC. Sex differences in cancer driver genes and biomarkers. *Cancer Res*. 2018;78(19):5527-5537.
5. Wilson MA, Buetow KH. Novel mechanisms of cancer emerge when accounting for sex as a biological variable. *Cancer Res*. 2020;80(1):27-29.
6. Burton A, Mohan S, Puplampu-Dove Y, Tse T. Characterizing gender eligibility descriptions for clinical trials registered on ClinicalTrials.gov. *JAMA*. 2023;330(20):2019-2021.
7. Ozdemir BC, Csajka C, Dotto GP, Wagner AD. Sex differences in efficacy and toxicity of systemic treatments: An undervalued issue in the era of precision oncology. *J Clin Oncol*. 2018;36(26):2680-2683.
8. Pala L, De Pas T, Conforti F. Under-representation of women in randomized clinical trials testing anticancer immunotherapy may undermine female patients care. A call to action. *Semin Oncol*. 2022;49(5):400-404.
9. Yuan Y, Liu L, Chen H, et al. Comprehensive characterization of molecular differences in cancer between male and female patients. *Cancer Cell*. 2016;29(5):711-722.
10. Kim AM, Tingen CM, Woodruff TK. Sex bias in trials and treatment must end. *Nature*. 2010;465(7299):688-689.
11. Lopes-Ramos CM, Quackenbush J, DeMeo DL. Genome-wide sex and gender differences in cancer. *Front Oncol*. 2020;10:597788.
12. Xiao T, Lee J, Gauntner TD, Velegraki M, Lathia JD, Li Z. Hallmarks of sex bias in immuno-oncology: mechanisms and therapeutic implications. *Nat Rev Cancer*. 2024;24(5):338-355.
13. Eksteen C, Riedemann J, van der Merwe FH, Botha MH, Engelbrecht AM. Advancing personalized medicine in LMICs: predictive indicators for cervical cancer immunotherapy response. *Semin Oncol*. 2025;52(4):152352.
14. Yan L, Liu Y, Zhang Z, Du F. Worldwide research trends on the immunotherapy-based treatment of ovarian cancers: A bibliometric and visual analysis. *J Multidiscip Healthc*. 2025;18:4197-4217.
15. Xiao Y, Yu X, Wang Y, et al. A novel immune-related gene signature for diagnosis and potential immunotherapy of microsatellite stable endometrial carcinoma. *Sci Rep*. 2024;14(1):3738.
16. Cristescu R, Mogg R, Ayers M, et al. Pan-tumor genomic biomarkers for PD-1 checkpoint blockade-based immunotherapy. *Science*. 2018;362(6411):eaar3593.
17. Zamarin D, Burger RA, Sill MW, et al. Randomized phase II trial of nivolumab versus nivolumab and ipilimumab for recurrent or persistent ovarian cancer: An NRG oncology study. *J Clin Oncol*. 2020;38(16):1814-1823.
18. Colombo N, Dubot C, Lorusso D, et al. Pembrolizumab for persistent, recurrent, or metastatic cervical cancer. *N Engl J Med*. 2021;385(20):1856-1867.
19. Luo PH, Mo DC, Wang HL, Liang XJ, Huang JF. Predicted value of PD-L1 for patients with cervical cancer treated with pembrolizumab. *J Clin Oncol*. 2024;42(13):1596.
20. Proppe L, Jagomast T, Beume S, et al. Prognostic and clinical heterogeneity of PD1 and PD-L1- immunohistochemical scores in endometrial cancers. *Arch Gynecol Obstet*. 2025;311(5):1395-1405.
21. Kaya M, Schaddelee MCA, Creutzberg CL, Kroep JR, Horeweg N. Efficacy of PD-(L)1 inhibition in the treatment of endometrial cancer across molecular classes: a systematic review and meta-analysis. *Int J Gynecol Cancer*. 2025;35(6):101759.
22. Zehir A, Benayed R, Shah RH, et al. Mutational landscape of metastatic cancer revealed from prospective clinical sequencing of 10,000 patients. *Nat Med*. 2017;23(6):703-713.
23. Zhang J, Bajari R, Andric D, et al. The international cancer genome consortium data portal. *Nat Biotechnol*. 2019;37(4):367-369.
24. Goldman MJ, Craft B, Hastie M, et al. Visualizing and interpreting cancer genomics data via the Xena platform. *Nat Biotechnol*. 2020;38(6):675-678.
25. Cerami E, Gao J, Dogrusoz U, et al. The cBio cancer genomics portal: an open platform for exploring multidimensional cancer genomics data. *Cancer Discov*. 2012;2(5):401-404.
26. Gao J, Aksoy BA, Dogrusoz U, et al. Integrative analysis of complex cancer genomics and clinical profiles using the cBioPortal. *Sci Signal*. 2013;6(269):pl1.
27. Ouyang J, Qin G, Liu Z, Jian X, Shi T, Xie L. ToPP: tumor online prognostic analysis platform for prognostic feature selection and clinical patient subgroup selection. *iScience*. 2022;25(5):104190.
28. Ozhan A, Tombaz M, Konu O. SmulTCan: A shiny application for multivariable survival analysis of TCGA data with gene sets. *Comput Biol Med*. 2021;137:104793.
29. Chandrashekar DS, Bashel B, Balasubramanya SAH, et al. UALCAN: A portal for facilitating tumor subgroup gene expression and survival analyses. *Neoplasia*. 2017;19(8):649-658.
30. Brunner M, Mullen L, Jauk F, et al. Automatic integration of clinical and genetic data using cBioPortal. *Stud Health Technol Inform*. 2022;290:799-803.
31. Kassambara A, Kosinski M. survminer: Drawing Survival Curves using "ggplot2". Comprehensive R Archive Network (CRAN). 2024.
32. Blanche P, Dartigues JF, Jacqmin-Gadda H. Review and comparison of ROC curve estimators for a time-dependent outcome with marker-dependent censoring. *Biom J*. 2013;55(5):687-704.
33. Vickers AJ, Van Calster B, Wynants L, Steyerberg EW. Correction: decision curve analysis: confidence intervals and hypothesis testing for net benefit. *Diagn Progn Res*. 2025;9(1):8.
34. Han Y, Wang Y, Dong X, et al. TISCH2: expanded datasets and new tools for single-cell transcriptome analyses of the tumor microenvironment. *Nucleic Acids Res*. 2023;51(D1):D1425-D1431.
35. Hao Y, Hao S, Andersen-Nissen E, et al. Integrated analysis of multimodal single-cell data. *Cell*. 2021;184(13):3573-3587.e3529.
36. Luca BA, Steen CB, Matusiak M, et al. Atlas of clinically distinct cell states and ecosystems across human solid tumors. *Cell*. 2021;184(21):5482-5496.e5428.

37. DepMap Consortium. DepMap Portal. 2025. https://depmap.org/portal
38. Chakravarty D, Gao J, Phillips SM, et al. OncoKB: a precision oncology knowledge base. *JCO Precis Oncol*. 2017;2017:1-16.
39. Sondka Z, Bamford S, Cole CG, Ward SA, Dunham I, Forbes SA. The COSMIC cancer gene census: describing genetic dysfunction across all human cancers. *Nat Rev Cancer*. 2018;18(11):696-705.
40. Frampton GM, Fichtenholtz A, Otto GA, et al. Development and validation of a clinical cancer genomic profiling test based on massively parallel DNA sequencing. *Nat Biotechnol*. 2013;31(11):1023-1031.
41. Vogelstein B, Papadopoulos N, Velculescu VE, Zhou S, Diaz LA Jr, Kinzler KW. Cancer genome landscapes. *Science*. 2013;339(6127):1546-1558.
42. Medgenome. 2024. https://oncokb.medgenome.com
43. Kim HW, Kim JH, Lim BJ, et al. Sex disparity in gastric cancer: female sex is a poor prognostic factor for advanced gastric cancer. *Ann Surg Oncol*. 2016;23(13):4344-4351.
44. Popejoy AB, Fullerton SM. Genomics is failing on diversity. *Nature*. 2016;538(7624):161-164.
45. Spratt DE, Chan T, Waldron L, et al. Racial/ethnic disparities in genomic sequencing. *JAMA Oncol*. 2016;2(8):1070-1074.
46. Cancer Genome Atlas Research N, Kandoth C. Integrated genomic characterization of endometrial carcinoma. *Nature*. 2013;497(7447):67-73.
47. Talhouk A, McConechy MK, Leung S, et al. A clinically applicable molecular-based classification for endometrial cancers. *Br J Cancer*. 2015;113(2):299-310.
48. León-Castillo A, de Boer SM, Powell ME. Molecular classification of the PORTEC-3 trial for high-risk endometrial cancer: impact on prognosis and benefit from adjuvant therapy. *J Clin Oncol*. 2020;38(29):3388-3397.
49. Tothill RW, Tinker AV, George J, et al. Novel molecular subtypes of serous and endometrioid ovarian cancer linked to clinical outcome. *Clin Cancer Res*. 2008;14(16):5198-5208.
50. Verhaak RG, Tamayo P, Yang JY, et al. Prognostically relevant gene signatures of high-grade serous ovarian carcinoma. *J Clin Invest*. 2013;123(1):517-525.
51. Cancer Genome Atlas Research N. Integrated genomic and molecular characterization of cervical cancer. *Nature*. 2017;543(7645):378-384.
52. Mollaoglu G, Brown BD, Baccarini A. Spatial genomics uncovers cytokines promoting ovarian tumour heterogeneity and immunotherapy resistance. *Clin Transl Med*. 2025;15(2):e70248.
53. Zhao F, Jiang X, Li Y, et al. Characterizing tumor biology and immune microenvironment in high-grade serous ovarian cancer via single-cell RNA sequencing: insights for targeted and personalized immunotherapy strategies. *Front Immunol*. 2024;15:1500153.
54. Wang ZB, Zhang X, Fang C, et al. Immunotherapy and the ovarian cancer microenvironment: exploring potential strategies for enhanced treatment efficacy. *Immunology*. 2024;173(1):14-32.
55. Zhang X, Wang Y, Gari A, Qu C, Chen J. Pan-cancer analysis of PARP1 alterations as biomarkers in the prediction of immunotherapeutic effects and the Association of its expression levels and immunotherapy signatures. *Front Immunol*. 2021;12:721030.
56. Mariathasan S, Turley SJ, Nickles D, et al. TGFbeta attenuates tumour response to PD-L1 blockade by contributing to exclusion of T cells. *Nature*. 2018;554(7693):544-548.
57. Dominguez CX, Muller S, Keerthivasan S, et al. Single-cell RNA sequencing reveals stromal evolution into LRRC15(+) myofibroblasts as a determinant of patient response to cancer immunotherapy. *Cancer Discov*. 2020;10(2):232-253.
58. Kieffer Y, Hocine HR, Gentric G, et al. Single-cell analysis reveals fibroblast clusters linked to immunotherapy resistance in cancer. *Cancer Discov*. 2020;10(9):1330-1351.
59. 10x Genomics. Support Portal. 2025. https://www.10xgenomics.com/support
60. Huang H, Weng H, Sun W, et al. Recognition of RNA N(6)-methyladenosine by IGF2BP proteins enhances mRNA stability and translation. *Nat Cell Biol*. 2018;20(3):285-295.

SUPPORTING INFORMATION

Additional supporting information can be found online in the Supporting Information section at the end of this article.

How to cite this article: Cuello MA, Gómez-Valenzuela F, Wichmann I, Kato S, Ibañez C. A sex-informed transcriptomic prognostic score for gynecologic cancers: Multiplatform validation and spatial characterization. *Int J Gynecol Obstet*. 2025;00:1-16. doi:10.1002/ijgo.70650